*Acta Cryst.* (1998). B54, 41–49

# Intermolecular Force-Field Parameters for Boron Hydrides

DONALD E. WILLIAMS* AND DAQUAN GAO

*Department of Chemistry, University of Louisville, Louisville, KY 40292, USA.*
*E-mail: dew01@xray5.chem.louisville.edu*

(*Received 28 May 1997; accepted 15 September 1997*)

## Abstract

Intermolecular atom–atom force-field parameters of the (exp-6-1) type for B and H atoms in boron hydrides were determined. They were obtained by full-weighted least-squares minimization of 116 forces in 15 observed crystal structures of boranes, the heat of sublimation of $B_{10}H_{14}$ and data from *ab initio* wavefunction calculations for diborane. Net atomic charges were obtained by fitting them to molecular electric potentials calculated from *ab initio* wavefunctions. Charges of terminal hydrogens were usually negative and those of bridging hydrogens usually positive. Repulsion-energy calculations for the $B_2H_6$ dimer provided the exponential dependence of H···H repulsion. Using the resulting force field, minimum-energy crystal structures were found with structural parameter values close to those of the observed structures. For diborane, energy minimization beginning with randomly oriented molecules placed initially in an 8 × 8 × 8 body-centered orthogonal cell led to the observed crystal structure and monoclinic space group.

## 1. Introduction

Although numerous sets of nonbonded interatomic potential parameters have been published for hydrocarbons and other organic molecules, little attention has been directed toward the boranes. A diverse assortment of borane molecules $B_nH_m$ is known and the structures of these molecules in many respects parallel structures of hydrocarbons. Nonbonded interatomic potential parameters for boron are still not well established. There has been a suggestion that hydrocarbon parameters can be used to simulate the borane crystal packing (Beringhelli *et al.*, 1983). In view of boron's smaller number of electrons and its very different bonding behavior, it seems unlikely that the nonbonded interaction of this element can be represented accurately by a C···C potential. Also, in contrast to hydrocarbons, there are two chemically different types of hydrogens in boranes, terminal and bridging.

In this work optimized nonbonded interatomic potential parameters for boron–boron and hydrogen–hydrogen interactions were obtained by fitting them to 116 forces in the observed crystal structures of 15 boranes, the heat of sublimation of $B_{10}H_{14}$ and to *ab initio* wavefunction data for diborane.

## 2. Intermolecular energy model

The nonbonded interaction of boron and hydrogen in boranes was modeled by pairwise additive interatomic functions of the (exp-6-1) type. Thus, the energy of interaction of two atoms in different molecules is given by

$$E(r_{jk}) = \alpha_j\alpha_k \exp(-0.5(\beta_j + \beta_k)r_{jk}) - \gamma_j\gamma_k r_{jk}^{-6} + \delta_j\delta_k r_{jk}^{-1},$$

where $\alpha$, $\beta$, $\gamma$ and $\delta$ are adjustable potential parameters and $r_{jk}$ is the distance between atom $j$ and atom $k$ in different molecules. The first term is intended to represent the exchange repulsion energy, the second dispersion attraction and the third Coulomb's law between net atomic charges. This equation implies a geometric mean combining law for hetero interactions. Thus, for the boranes there are eight potential parameters to be determined: $\alpha$, $\beta$, $\gamma$ and $\delta$ for B and H atoms. An attempt to subdivide hydrogens into terminal (H*t*) and bridging (H*b*) types was judged not necessary. The $\delta$ parameters were set externally by the potential-derived method (PD net atomic charges); the $\gamma$ parameters were set externally by QM (quantum mechanical) repulsion calculations. This leaves four parameters to be determined from crystal data (six if hydrogens are subdivided into H*t* and H*b*).

The crystal energy was calculated by making a lattice summation over all $r_{jk}$ between atoms in the asymmetric unit (usually one molecule) and atoms of surrounding molecules. A distance cutoff of 12 Å was used. Accelerated convergence was used to increase the accuracy of the dispersion and Coulomb energies (Williams, 1971).

The adjustable parameters $\alpha$ and $\beta$ of the exchange repulsion energy formula are highly correlated. In the crystal-structure-based optimizations discussed below it was difficult to optimize them simultaneously. A strategy was adopted which used linear extrapolation from carbon and neon to obtain a reasonable value for boron $\beta$. Experimentally derived $\beta$ values for carbon and neon have been obtained from crystal structures of graphite and neon, heats of sublimation and compressibility data

(Crowell, 1958; Williams, 1972). Table 1 shows linear interpolated (*versus* atomic number) values of repulsion exponents $\beta$ assigned for the series boron to neon. An extrapolated value of 3.42 $Å^{-1}$ was adopted for the exponential dependence of B···B repulsion. The interpolated values for N, O and F have been used previously for azahydrocarbons (Williams & Cox, 1984), oxohydrocarbons (Cox *et al.*, 1981) and perfluorocarbons (Williams & Houpt, 1986).

Table 1. *Repulsion exponents for some second-row elements* ($Å^{-1}$)

| Element | B | C | N | O | F | Ne |
|---|---|---|---|---|---|---|
| $\beta$ value | 3.42 | 3.60† | 3.78 | 3.96 | 4.16 | 4.36† |

† Experimentally derived value.

## 3. Structure of diborane

The simplest borane molecule, $B_2H_6$, was selected for evaluation of the repulsion exponential dependence of the H···H interaction. In this molecule there are four terminal hydrogens, H*t*, and two bridging hydrogens, H*b*. As an initial step the diborane structure was optimized using the *Gaussian*92 computer program (Frisch *et al.*, 1992) at the HF/6-31G** level. Table 2 compares the quantum mechanical optimized structure to the experimental structure measured in the gas (Duncan & Harper, 1984) and in the crystal (Smith & Lipscomb, 1965). The QM result agrees quite well with the experimentally determined gas phase structure. The crystal structure work, carried out under difficult experimental conditions, appears to be less accurate. Note that *X*—H bond distances observed by X-ray diffraction are normally foreshortened by 0.07–0.10 Å, because of the relatively large bonding electron shift of hydrogen electron density (Starr & Williams, 1977).

Table 2. *Calculated and observed structure of diborane* (*Å*,°)

| | QM | Gas | Solid |
|---|---|---|---|
| B—H*t* | 1.1845 | 1.184 (3) | 1.09 (2) |
| B—H*b* | 1.3166 | 1.314 (3) | 1.24 (2) |
| H*t*—B—H*t* | 121.98 | 121.5 (5) | 124 (1) |
| H*b*—B—H*b* | 95.08 | 96.9 (5) | 90 (1) |

## 4. Intermolecular repulsion in diborane dimer

As mentioned above, the exponent parameters of (exp-6-1) nonbonded interatomic potentials are difficult to obtain from crystal structure data; the setting of the exponent value for boron was discussed above. To obtain H-atom exponent parameters for boranes we utilized intermolecular energy from QM calculations on the $B_2H_6$ dimer. These calculations were on the Hartree–Fock level with the same 6-31G** basis set. Hartree–Fock calculations do not include any dispersion energy, so the intermolecular energy can be modeled with repulsion and coulombic functions alone.

Three configurations were considered: one which emphasizes the H*t*···H*t* interaction (Fig. 1*a*), a side-by-side placement in which the H*b*···H*b* distance is the closest intermolecular contact (Fig. 1*b*) and a side-by-side twisted model in which the two rings of the molecules are perpendicular to each other and displaced (Fig. 1*c*). The intermolecular energy is $\Delta E = E_2 - 2E_1$, where $E_2$ is the energy of the dimer and $E_1$ is the energy of the monomer calculated with the same dimer basis set (basis set superposition corrected energy). The optimized structure as described previously was used as the monomer structure.

$\Delta E$ was decomposed into $E$(rep) + $E$(coul), where $E$(coul) is the coulombic interaction energy between the two molecules which was represented by a net atomic charge model; $E$(rep) is the repulsion energy. The assignment of net atomic charges for the boranes is discussed in the following section. For diborane, these charges are (in units of absolute electronic charge): B, 0.1414; H*t*, −0.1038; H*b*, 0.0644. After subtraction of the coulombic energy, the repulsion energy can be modeled by the sum of the atom–atom exponential potential functions, $E_{jk}(\text{rep}) = \alpha_j\alpha_k \exp(-0.5(\beta_j + \beta_k)r_{jk})$. $E$(rep) is obtained by summation over all the intermolecular $j$, $k$ pairs. The $\beta$ parameter for boron was set as described above; least-squares fitted values were obtained for $\alpha^2$ for B; both $\alpha^2$ and $\beta$ values were found for two types of hydrogen (five adjustable parameters). The resulting potential functions are B···B: $\alpha^2$ = 247 155 kJ $mol^{-1}$, $\beta$ = 3.42 $Å^{-1}$ (assumed); H*t*···H*t* $\alpha^2$ = 8547.28 kJ $mol^{-1}$, $\beta$ = 3.59 $Å^{-1}$; H*b*···H*b* $\alpha^2$ = 3177.75 kJ $mol^{-1}$, $\beta$ = 3.32 $Å^{-1}$.

The two repulsion-only functions for hydrogens are illustrated in Fig. 2, labeled as H*t*···H*t*(QM) and

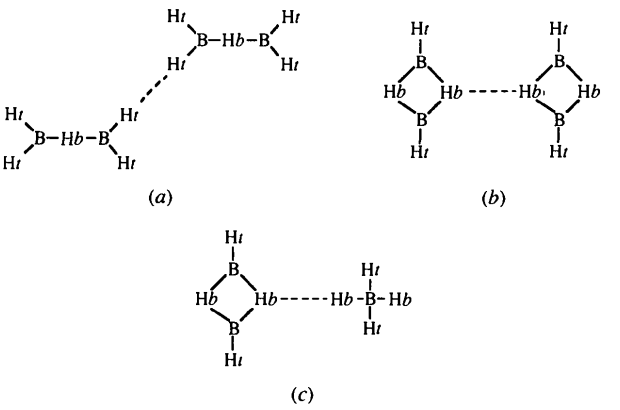


Fig. 1. Three orientations of the diborane dimer.

H*b*···H*b*(QM). Since repulsion arises from electron density overlap of filled orbitals, which is prohibited by the Pauli exclusion principle, it is reasonable that negatively charged H*t* should be more repulsive than positively charged H*b*. Hydrogen is most sensitive to modification of its repulsion, since a net charge of −0.1 electrons on H*t*, for example, represents a 10% increase in electron count. The fitting results also indicate that H*b*, with its positive charge and lower electron count, has a potential with a smaller exponent than H*t*. Therefore, the fitting results indicate that, in addition to being smaller, H*b* is also softer than H*t*. The repulsion-only function obtained for B···B is illustrated in Fig. 3, labeled as B···B(2H,QM).

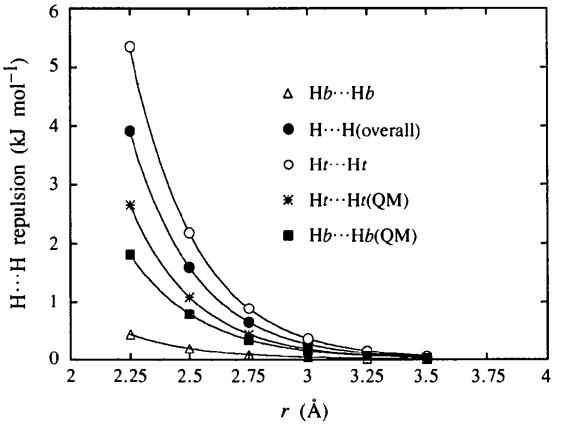


Fig. 2. H···H repulsion-only energies. The asterisk and square marked curves were obtained by fitting the quantum mechanical repulsion energy of the diborane dimer. The solid circle marked curve was obtained from borane crystal data, assuming one type of hydrogen; open circle and triangle marked curves are from crystal data, assuming two types of hydrogen.

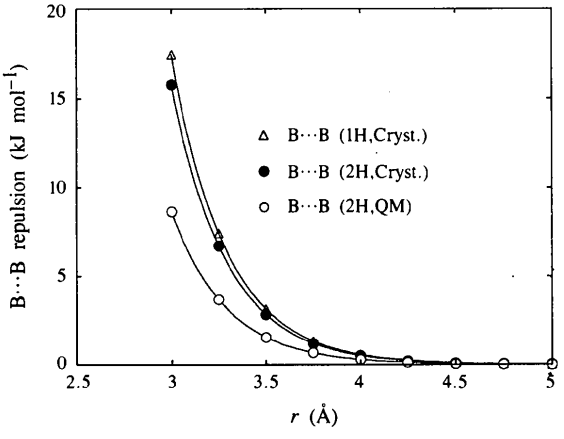


Fig. 3. B···B repulsion-only energies. The open circle marked curve was obtained by fitting the quantum mechanical repulsion energy of the diborane dimer. The triangle marked curve was obtained from borane crystal data, assuming one type of hydrogen; the solid circle marked curve was obtained from crystal data, assuming two types of hydrogen.

## 5. Potential-derived net atomic charges

The *Gaussian*92 package (Frisch *et al.*, 1992) was utilized to calculate the molecular electric potential in the van der Waals envelopes of the borane molecules. Except for diborane (which was optimized as described above), atomic coordinates were taken from the observed crystal structures. The wavefunctions were of HF/6-31G** quality. The MEP was evaluated at geodesic grid points (Spackman, 1996) with the following parameters: icosahedral fourfold tesselation; first layer of points at 1.6 times the van der Waals radius; five layers with 0.2 Å spacing. The recipe yielded 1000–2700 MEP grid points per molecule, depending on the size of the molecule. The van der Waals radii of hydrogen and boron were taken as 1.2 and 1.8 Å.

The program *pdm*97 (Williams, 1997*a*) was used to fit net atomic charges (PD charges) to the MEP; r.m.s. (root mean square) and r.r.m.s. (relative root mean square) fits are shown in Table 3. The r.r.m.s. values ranged from 2.9 to 19.0% with the better fits obtained with large borane molecules and the poorer fits obtained with small borane molecules, especially diborane.

## 6. Crystal structure data for boranes

A search of the 1996 Cambridge Structural Database (Allen & Kennard, 1993) located 17 borane crystal structures. 15 of these structures were selected for derivation of the force field; crystal structure data is given in Table 3 and the molecular structures are shown in Fig. 4. Note that there are three isomers of icosaborane(26) which crystallize in three different space groups. The structure of $B_9H_{15}$ (Dickerson *et al.*, 1957) was not used because of a discrepancy between the reported $B^V$—$B^{VI}$ distance and the value calculated from the reported atomic coordinates. The structure of $B_{12}H_{16}$ (Brewer *et al.*, 1985) was not used because of a suspect misplaced H atom.

All the crystal structures were determined by X-ray diffraction, which fundamentally determines electron density, not nuclear positions. For boron, the peak of electron density almost exactly coincides with the nuclear position. However, for hydrogen the peak of electron density is appreciably shifted into the bond (Starr & Williams, 1977). In boranes this electron density shift is quite noticeable for terminal hydrogens. In diborane the observed B—H*t* X-ray distance is 1.09 ± 0.02, while the QM optimized value is 1.18 Å. The present force field is based on X-ray hydrogen positions, *i.e.* foreshortened B—H*t* bonds. X-ray positions were also used for H*b*, a type of bond where the bonding electron shift has not been investigated.

## 7. Derivation of intermolecular force-field parameters

At equilibrium, all forces in the crystal are zero. If the crystal has one rigid molecule in the asymmetric unit, the

Table 3. *Data for borane crystals*

| Name | Diborane | Tetraborane | Pentaborane(9) |
|---|---|---|---|
| Formula | $B_2H_6$ | $B_4H_{10}$ | $B_5H_9$ |
| Filename | b2h6 | b4h10 | b5h9 |
| Space group | $P2_1/n$ | $P2_1/n$ | $I4_1/acd$ |
| $Z$ | 2 | 4 | 2 |
| Temperature (K) | 83 | 298 | 158 |
| R.m.s. (kJ mol$^{-1}$) | 1.5 | 2.0 | 2.5 |
| R.r.m.s. (%) | 19.0 | 16.8 | 10.2 |
| No. of forces | 7 | 10 | 2 |
| $R_F$ (kJ mol$^{-1}$ Å$^{-1}$) | 1.95 | 0.42 | 0.12 |
| Reference | (*a*) | (*b*) | (*c*) |

| Name | Pentaborane(11) | Octaborane | Decaborane |
|---|---|---|---|
| Formula | $B_5H_{11}$ | $B_8H_{12}$ | $B_{10}H_{14}$ |
| Filename | b5h11 | b8h12 | b10h14 |
| Space group | $P2_1/n$ | $Pbca$ | $C2/c$ |
| $Z$ | 4 | 8 | 8 |
| Temperature (K) | 133 | 173 | 113 |
| R.m.s. (kJ mol$^{-1}$) | 1.4 | 1.3 | 1.3 |
| R.r.m.s. (%) | 7.1 | 5.4 | 4.8 |
| No. of forces | 10 | 9 | 8 |
| $R_F$ (kJ mol$^{-1}$ Å$^{-1}$) | 4.66 | 0.26 | 1.03 |
| Reference | (*b*) | (*d*) | (*e*) |

| Name | Tridecaborane | Tetradecaborane | Hexadecaborane |
|---|---|---|---|
| Formula | $B_{13}H_{19}$ | $B_{14}H_{20}$ | $B_{16}H_{20}$ |
| Filename | b13h19 | b14h20 | b16h20 |
| Space group | $P2_1/c$ | $P2_12_12_1$ | $P2_1/c$ |
| $Z$ | 4 | 4 | 4 |
| Temperature (K) | 298 | 109 | 295 |
| R.m.s. (kJ mol$^{-1}$) | 1.0 | 1.0 | 1.0 |
| R.r.m.s. (%) | 3.8 | 3.4 | 4.8 |
| No. of forces | 10 | 9 | 10 |
| $R_F$ (kJ mol$^{-1}$ Å$^{-1}$) | 1.07 | 0.90 | 1.17 |
| Reference | (*f*) | (*g*) | (*h*) |

| Name | Octadecaborane | Iso-octadecaborane | Icosaborane(16) |
|---|---|---|---|
| Formula | $B_{18}H_{22}$ | $B_{18}H_{22}$ | $B_{20}H_{16}$ |
| Filename | b18h22 | b18h22iso | b20h16 |
| Space group | $Pccn$ | $P2_1/c$ | $I4_1/acd$ |
| $Z$ | 4 | 4 | 8 |
| Temperature (K) | 295 | 298 | 295 |
| R.m.s. (kJ mol$^{-1}$) | 0.9 | 1.0 | 0.7 |
| R.r.m.s. (%) | 5.9 | 4.9 | 8.2 |
| No. of forces | 6 | 10 | 3 |
| $R_F$ (kJ mol$^{-1}$ Å$^{-1}$) | 1.30 | 1.28 | 2.31 |
| Reference | (*i*) | (*j*) | (*k*) |

| Name | Icosaborane(26) | Icossaborane(26) | Icosaborane(26) |
|---|---|---|---|
| Formula | $B_{20}H_{26}$ | $B_{20}H_{26}$ | $B_{20}H_{26}$ |
| Filename | 15b20h26 | 22b20h26 | 26b20h26 |
| Space group | $P2_1/n$ | $I4_1/acd$ | $Pbca$ |
| $Z$ | 4 | 8 | 8 |
| Temperature (K) | 295 | 298 | 298 |
| R.m.s. (kJ mol$^{-1}$) | 0.9 | 0.9 | 0.9 |
| R.r.m.s. (%) | 3.3 | 3.7 | 2.9 |
| No. of forces | 10 | 3 | 9 |
| $R_F$ (kJ mol$^{-1}$ Å$^{-1}$) | 0.77 | 1.36 | 3.55 |
| Reference | (*l*) | (*m*) | (*m*) |

(*a*) Smith & Lipscomb (1965); (*b*) Moore *et al.* (1957); (*c*) Dulmage & Lipscomb (1952); (*d*) Enrione *et al.* (1964); (*e*) Brill *et al.* (1971); (*f*) Huffman *et al.* (1976); (*g*) Huffman *et al.* (1981); (*h*) Friedman *et al.* (1970); (*i*) Simpson & Lipscomb (1963); (*j*) Simpson *et al.* (1963); (*k*) Dobrott *et al.* (1964); (*l*) Brown *et al.* (1979); (*m*) Boocock *et al.* (1980).

intermolecular degrees of freedom are six lattice constants, three rotations and three translations of the molecule in the unit cell. The correct intermolecular force field will yield zero forces for each of these degrees of freedom. The symmetry of the unit cell may reduce the degrees of freedom. For example, monoclinic cells have only one variable angle and tetragonal cells have only two independent cell edge lengths. If the number of molecules per cell, $Z$, is less than the number of space-group operations, the molecule must lie on a symmetry element. In this case some rotations and/or translations are not allowed. For example, a molecule on a twofold axis in the $y$ direction can only rotate around and translate along $y$. If there is more than one molecule in the asymmetric unit, six degrees of freedom are added for each additional molecule. All of these types of symmetry are encountered in the borane crystal data set. Table 3 shows the number of independent forces in each crystal.

The method of force-field derivation has been described previously (Hsu & Williams, 1980) and is implemented with the *nbp* (for nonbonded parameters) computer program (Williams, 1997*b*). The full-weight matrix force minimization method was used, which defines a residual function

$$R = \Sigma_{\text{structures}}(R_F + R_E),$$

where $R_F(q_i) = \Sigma_j \Sigma_k w_{jk} F_j(p_j^0, q_i) F_k(p_k^0, q_i)$ and

$$R_E(q_i) = w'(E_{\text{lattice}} - \Delta H_{\text{subl}})^2.$$

The $p_j^0$ are observed generalized structural parameters; $q_i$ are generalized potential parameters; $F_j$ is the $j$th generalized force for the structure, which is the negative first derivative of the lattice energy with respect to $p_j$. The forces, like the calculated lattice energies, are obtained by lattice summation over the crystal structure. The weight

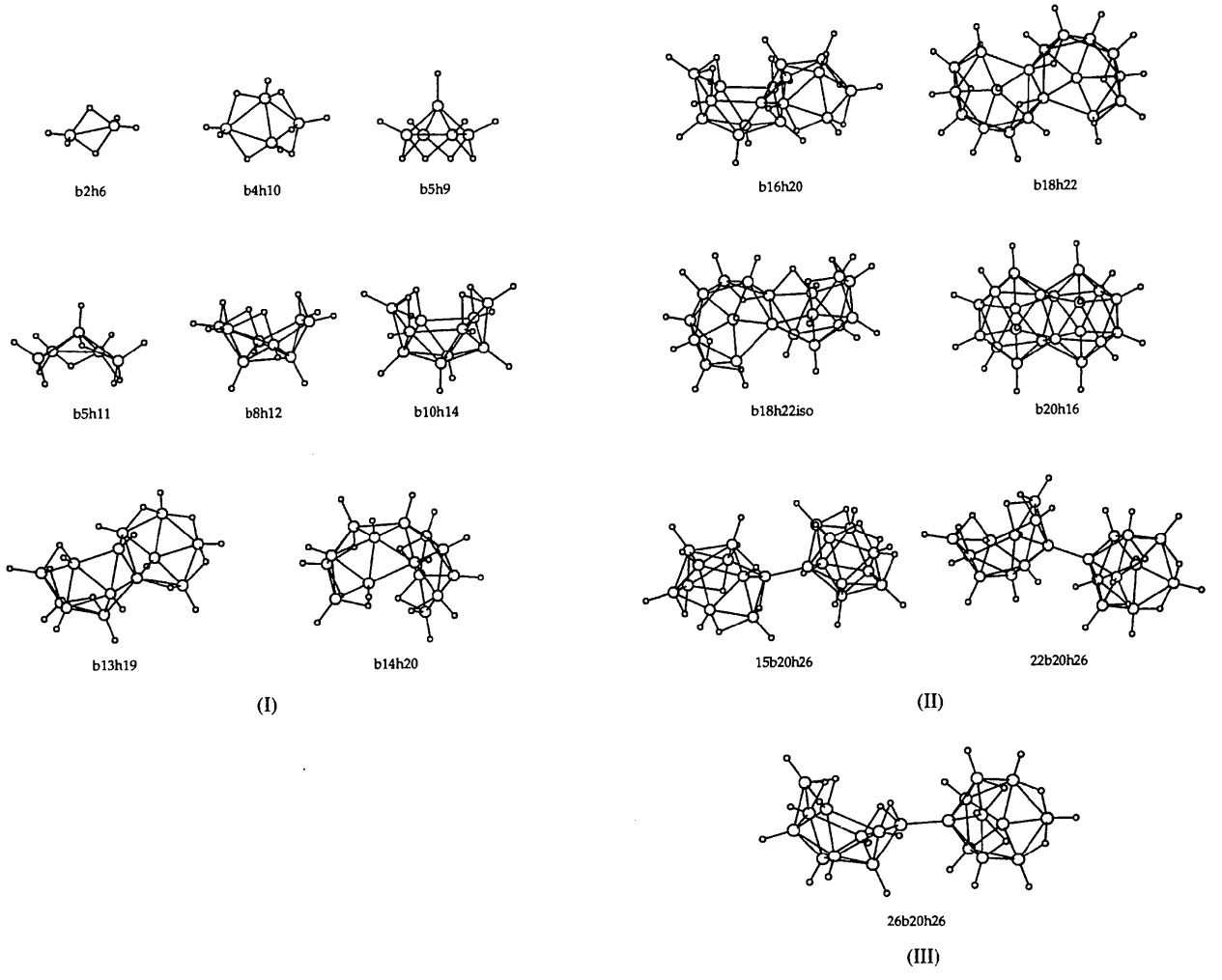


Fig. 4. Borane molecular structures.

Table 4. *Structural shifts obtained with this force field*

Energies (kJ mol$^{-1}$) are shown for the observed and replaced structures.

| Filename | $\Delta a$ (%) | $\Delta b$ (%) | $\Delta c$ (%) | $\Delta\beta$ (°) | Rotation (°) | Translation (Å) | $E_{obs}$ | $E_{min}$ |
|---|---|---|---|---|---|---|---|---|
| b2h6 | −0.1 | 6.2 | −1.1 | 1.0 | 3.0 | | −16.23 | −16.87 |
| b4h10 | 0.4 | −1.0 | 2.0 | 3.1 | 1.2 | 0.11 | −32.51 | −33.25 |
| b5h9 | −0.1 | −0.1 | 1.7 | | | | −41.44 | −41.62 |
| b5h11 | 2.1 | 0.9 | −1.6 | 3.2 | 1.4 | 0.18 | −40.55 | −42.06 |
| b8h12 | −0.8 | −0.4 | −0.2 | | 0.8 | 0.03 | −66.89 | −67.36 |
| b10h14 | 1.8 | 4.1 | −0.5 | 0.1 | 0.3† | 0.22† | −76.00‡ | −79.62 |
| b13h19 | −1.8 | −1.4 | 1.0 | 0.6 | 1.6 | 0.18 | −96.56 | −97.99 |
| b14h20 | 2.1 | 1.4 | −1.4 | | 3.2 | 0.13 | −100.32 | −102.04 |
| b16h20 | 0.5 | −2.2 | 0.1 | 1.2 | 1.5 | 0.08 | −110.63 | −111.55 |
| b18h22 | 1.8 | −0.7 | 1.7 | | 2.4 | | −121.39 | −123.16 |
| b18h22iso | −1.9 | −0.6 | −1.3 | −0.2 | 0.8 | 0.15 | −125.25 | −127.28 |
| b20h16 | −2.5 | | −0.7 | | 2.7 | | −139.97 | −144.79 |
| 15b20h26 | −1.5 | −0.8 | 1.0 | 1.7 | 0.5 | 0.23 | −134.91 | −136.78 |
| 22b20h26 | −0.3 | | −1.9 | | 0.1 | | −142.25 | −143.34 |
| 26b20h26 | −2.9 | 1.2 | −0.1 | | 1.6 | 0.09 | −139.83 | −142.35 |

† Average for two molecules in asymmetric unit. ‡ Fitted value.

matrix **w** is constructed from the Hessian **H** (second derivative matrix) and the variance matrix **V** (a diagonal matrix with elements of the error allowances on structural parameters)

$$\mathbf{w} = [\mathbf{H}^t \mathbf{V} \mathbf{H}]^{-1}.$$

$R_E$ is a penalty function which requires agreement with observed heats of sublimation. The weight $w'$ is adjusted to give the desired fit of the calculated crystal energy, $E_{lattice}$, with the observed heat of sublimation, $\Delta H_{subl}$. If $R_E$ is used for only one crystal structure (as in the present case) it can be regarded as a side condition which can be fitted exactly by scaling the potential parameters.

It is desirable to have several $\Delta H_{subl}$ to better define the potential parameters. In particular, several values can assist in the allocation of energy between atom types (Williams, 1967). However, for the borane training data set only one observed sublimation energy was found in the literature. The heat of sublimation of decaborane, $B_{10}H_{14}$, was obtained from vapor pressure data (Knacke *et al.*, 1991) as 76.0 kJ mol$^{-1}$.

To minimize $R$, a Taylor's expansion is performed on the forces and calculated lattice energies with respect to the potential parameters. A first-order approximation yields a set of linear equations for shifts $\Delta q_i$ (increments of the potential parameters between the current refinement cycle and the previous one). The resulting equations are solved for $\Delta q_i$. This process is iterated until convergence is reached.

In this work the forces in the crystal structures were minimized using observed crystal and molecular structures and PD net atomic charges. We also fixed the exponents for B···B and H···H interactions as 3.42 and 3.59 Å$^{-1}$. The four fitted potential parameters were two repulsion coefficients $\alpha$ and two dispersion coefficients $\gamma$ for boron and carbon. Hetero interactions were obtained by the geometric mean combining rule, as follows from the form of the potential. Table 3 gives minimized $R_F$ values for the 15 boranes corresponding to the optimized nonbonded interatomic potential functions

boron: $E = -4911.63r^{-6} + 391403.5 \exp(-3.42r)$ (Fig. 3, 1H, Cryst. curve);

hydrogen: $E = -58.30r^{-6} + 10821.5 \exp(-3.59r)$ (Fig. 2, H···H overall curve).

These are the recommended intermolecular potential functions for boranes. Note that repulsions found in the crystal are larger than those from the QM calculation of the diborane dimer. This is expected, since the QM calculation does not include any thermal motion or account for thermal expansion; however, the increase in apparent repulsion in the crystal is surprisingly large.

The final test of the force field determination was to relax the crystal structural parameters from their observed values to allow all forces to go to zero, that is, minimize the crystal energy with respect to the structural parameters. An energy minimum was always found near the observed starting structure. The resulting energies and structural shifts are shown in Table 4.

It is expected that an observed structure with large $R_F$ will show the largest shifts to the corresponding relaxed structure. Files b2h6, b5h11, b20h16 and 26b20h26 have the largest $R_F$ values of 1.95, 4.66, 2.31 and 3.55, respectively. Table 4 shows that b2h6 has the largest percentage shift in a cell edge, +6.2% along $b$. In the case of b5h11 relaxation shifts appear normal when using a force field with no explicit thermal information. The tetragonal b20h16 structure shows 2.5% contraction along two cell edges. Finally, the 26b20h26 relaxation shifts appear normal.

Viewed from the other direction, it is expected that a structure showing large relaxation shifts would have a large $R_F$. An exception was the b10h14 structure, which showed a 4.1% increase in the $b$ cell edge, even though

its $R_F$ is only 1.03. Attention is called to the fact that b10h14 is the only structure in the training set with more than one molecule (in fact, two) in the crystallographic asymmetric unit.

### 8. Separate potentials for H*t* and H*b*

One possible causal factor for the larger relaxation shifts could be the assumption of only one nonbonded potential for hydrogen. To check this hypothesis we repeated our force-field derivation, making allowance for separate hydrogen potentials for terminal and bridging hydrogens. For H*b* the repulsion exponent was taken as 3.32 $Å^{-1}$ from the diborane dimer quantum mechanical calculation. This increased the number of derived potential parameters from four to six. Of course, just adding the additional two variables would be expected to reduce the value of $R$. In fact, $R$ decreased from 22.14 to 14.50. However, the relaxation crystal structure shifts were not much smaller, consistent with the idea that most of the decrease in $R$ was simply caused by the increase in the number of potential variables.

For the case of two types of hydrogen, the derived potentials are

B: $E = -5323.89r^{-6} + 450618.4\exp(-3.42r)$ (Fig. 3, 2H, Cryst. curve)

H*t*: $E = -51.91r^{-6} + 12600.4\exp(-3.59r)$ (Fig. 2, H*t*···H*t* curve)

H*b*: $E = -10.87r^{-6} + 767.0\exp(-3.32r)$ (Fig. 2, H*b*···H*b* curve).

It seems likely that the large difference between the H*t* and H*b* potentials is an artifact accidentally introduced because of other features of the intermolecular potential model, *e.g.* neglect of thermal effects, higher-order dispersion terms, inadequacies of the net atomic charge model or repulsion model. *Therefore, we do not recommend the use of the borane intermolecular potential with two types of hydrogen.* Interestingly, the repulsion curves do depict H*t* larger than H*b*, which is consistent with the idea that the size of a bonded hydrogen increases with negative net atomic charge.

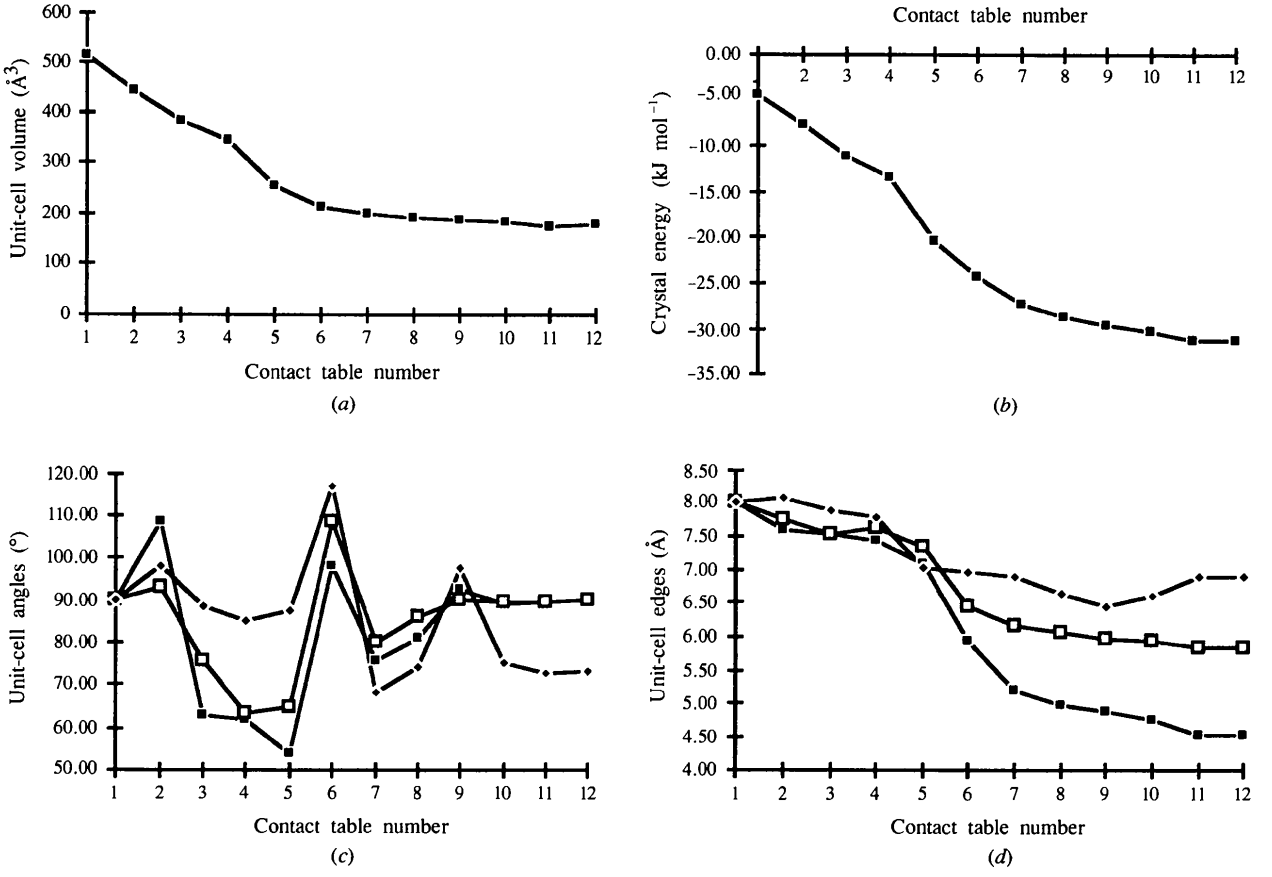


Fig. 5. (*a*) Unit-cell volume ($Å^3$) *versus* contact table number. (*b*) Crystal energy (kJ $mol^{-1}$) *versus* contact table number. (*c*) Unit-cell angles (°) *versus* contact table number. (*d*) Unit-cell edges (Å) *versus* contact table number.

### 9. *Ab initio* modeling of the diborane crystal structure

If the molecular structure is known, a sufficiently accurate force field should allow *ab initio* modeling of the crystal structure starting from a random model, including prediction of the space-group symmetry (Williams, 1996*a*). In practice, *ab initio* crystal modeling has proven difficult because of a multitude of subsidiary minima on the crystal energy hypersurface and inaccuracies in the force field. If a subsidiary energy minimum is close to the observed energy, polymorphism may be indicated. If a subsidiary energy minimum is lower than the observed energy and polymorphism is not present, force-field inaccuracies may be indicated. We used the computer program *mpa* [for molecular packing analysis (Williams, 1996*b*)] to test if the present force field could correctly model the crystal structure of diborane starting from low density initial structures.

The initial structures, which had very small packing energies, were formed by placing two QM optimized diborane molecules in a 8 × 8 × 8 Å cell. The molecules were rotated to initial orientations using points randomly selected from a Lattman angle grid. A Lattman angle grid (Williams, 1973) was used to provide a nearly uniform sampling of rotation space. During energy minimization no symmetry was assumed so that the calculation can be described as triclinic, space group $P1$, with two independent molecules in the cell. The first molecule was fixed at the cell origin and the second molecule was initially placed at the body center. The lattice energy was minimized with respect to the structural variables. The structural variables in this case are six cell constants plus three rotations of the origin molecule plus three translations and three rotations of the second molecule.

The initial model has much lower density than the solid phase, in fact, it resembles a dense gas with disordered molecular orientations. In the *mpa* program, a contact table of all nonbonded interatomic distances, up to the summation limit, is produced. Several iterations of energy minimization are made with this contact table. Then a new table is made and the process repeated until convergence is achieved. The summation limit and accelerated convergence parameters were the same as with the *nbp* calculation.

This calculation is Monte Carlo in nature and most energy minimizations led to subsidiary minima with higher energy than the observed. Fig. 5 shows the results of an *ab initio* calculation with $Z = 2$, which correctly modeled the observed crystal structure of diborane.

Fig. 5(*a*) shows that as the crystal energy is minimized the unit-cell volume smoothly decreases (and therefore the density increases). Fig. 5(*b*) shows the corresponding drop in the crystal energy. Since no symmetry was specified in the calculation, unit-cell angles immediately deviate from 90° and diverge widely until they eventually converge to monoclinic values near contact table 10 (Fig. 5*c*). Wide swings in the cell angles are caused by changes in the definition of the reduced unit cell. The cubic symmetry of the lattice constants quickly disappears but eventually they converge to the observed relaxed monoclinic values near contact table 11 (Fig. 5*d*). Examination of the model structure produced with contact table 12 shows that it is identical with the relaxed observed structure, including space-group symmetry $P2_1/n$.

We are grateful for financial support from The Petroleum Research Fund.

### References

Allen, F. H. & Kennard, O. (1993). *Chem. Des. Autom. News*, **8**, 31–37.

Beringhelli, T., Filippini, G., Gavezzotti, A. & Simonetta, M. (1983). *J. Mol. Struct.* **94**, 51–61.

Boocock, S. K., Greenwood, N. N., Kennedy, J. D., McDonald, W. S. & Staves, J. (1980). *J. Chem. Soc. Dalton Trans.* pp. 790–796.

Brewer, C. T., Swisher, R. G., Sinn, E. & Grimes, R. M. (1985). *J. Am. Chem. Soc.* **107**, 3558–3564.

Brill, R., Dietrich, H. & Dierks, H. (1971). *Acta Cryst.* B**27**, 2003–2018.

Brown, G. M., Pinson, J. W. & Ingram Jr, L. L. (1979). *Inorg. Chem.* **18**, 1951–1956.

Cox, S. R., Hsu, L. Y. & Williams, D. E. (1981). *Acta Cryst.* A**37**, 293–301.

Crowell, A. D. (1958). *J. Chem. Phys.* **29**, 446–447.

Dickerson, E. W., Wheatley, R. J., Howell, P. A. & Lipscomb, W. N. (1957). *J. Chem. Phys.* **27**, 200–209.

Dobrott, R. D., Friedman, L. B. & Lipscomb, W. N. (1964). *J. Chem. Phys.* **40**, 866–872.

Dulmage, W. J. & Lipscomb, W. N. (1952). *Acta Cryst.* **5**, 260–264.

Duncan, J. L. & Harper, J. (1984). *Mol. Phys.* **51**, 371–380.

Enrione, R. E., Boer, F. P. & Lipscomb, W. N. (1964). *Inorg. Chem.* **3**, 1659–1666.

Friedman, L. B., Cook, R. E. & Glick, M. D. (1970). *Inorg. Chem.* **9**, 1452–1458.

Frisch, M. J., Trucks, G. W., Head-Gordon, M., Gill, P. M. W., Wong, M. W., Foresman, J. B., Johnson, B. G., Schlegel, H. B., Robb, M. A., Replogle, E. S., Gomperts, R., Andres, J. L., Raghavachari, K., Binkley, J. S., Gonzalez, C., Martin, R. L., Fox, D. J., Defrees, D. J., Baker, J., Stewart, J. J. P., Pople, J. A. (1992). *Gaussian*92. Revision A. Gaussian, Inc., Pittsburgh PA.

Hsu, L.-Y. & Williams, D. E. (1980). *Acta Cryst.* A**36**, 277–281.

Huffman, J. C., Moody, D. C. & Schaeffer, R. (1976). *Inorg. Chem.* **15**, 227–232.

Huffman, J. C., Moody, D. C. & Schaeffer, R. (1981). *Inorg. Chem.* **20**, 741–745.

Knacke, O., Kubaschewski, O. & Hesselmann, K. (1991). *Thermochemical Properties of Inorganic Substances*, 2nd ed, p. 121. Berlin: Springer-Verlag.

Moore, E. B. Jr, Dickerson, R. E. & Lipscomb, W. N. (1957). *J. Chem. Phys.* **27**, 209–211.

Simpson, P. G., Folting, K., Dobrott, R. D. & Lipscomb, W. N. (1963). *J. Chem. Phys.* **39**, 2339–2348.

Simpson, P. G. & Lipscomb, W. N. (1963). *J. Chem. Phys.* **39**, 26–34.
Smith, H. W. & Lipscomb, W. N. (1965). *J. Chem. Phys.* **43**, 1060–1064.
Spackman, M. A. (1996). *J. Comput. Chem.* **17**, 1–18.
Starr, T. L. & Williams, D. E. (1977). *J. Chem. Phys.* **66**, 2054–2057.
Williams, D. E. (1967). *J. Chem. Phys.* **47**, 4680–4684.
Williams, D. E. (1971). *Acta Cryst.* A**27**, 452–455.
Williams, D. E. (1972). *Acta Cryst.* A**28**, 84–88.
Williams, D. E. (1973). *Acta Cryst.* A**29**, 408–414.
Williams, D. E. (1996*a*). *Acta Cryst.* A**52**, 326–328.
Williams, D. E. (1996*b*). *mpa/mpg. Molecular Packing Analysis and Molecular Packing Graphics*. Chemistry Department, University of Louisville, Louisville, KY 40292, USA.
Williams, D. E. (1997*a*). *pdm*97. *Potential-Derived Multipoles*. Chemistry Department, University of Louisville, Louisville, KY 40292, USA.
Williams, D. E. (1997*b*). *nbp. Derivation of Nonbonded Potential Parameters*. Chemistry Department, University of Louisville, Louisville, KY 40292, USA.
Williams, D. E. & Cox, S. R. (1984). *Acta Cryst.* B**40**, 404–417.
Williams, D. E. & Houpt, D. J. (1986). *Acta Cryst.* B**42**, 286–295.